https://doi.org/10.1016/j.fluid.2020.112657

Thermodynamic modeling of CO_2 solubility in saline water using NVT flash with the Cubic-Plus-Association equation of state

Yiteng Li[a], Zhonghua Qiao[b], Shuyu Sun[a,*], Tao Zhang[a]

[a] *Computational Transport Phenomena Laboratory (CTPL), Physical Science and Engineering Division (PSE), King Abdullah University of Science and Technology (KAUST), Thuwal 23955-6900, Saudi Arabia*

[b] *Department of Applied Mathematics, Hong Kong Polytechnic University, Hung Hom, Kowloon, Hong Kong*

Abstract

The accurate estimation of CO_2 sequestration potential in deep saline aquifers requires the knowledge of CO_2 solubility in brine, thus placing importance on reliable thermodynamic models that account for the effect of different salts and their mixtures over wide ranges of pressure, temperature and salt concentration. Most literature investigated CO_2 solubility in a single-salt solution as a replacement of real saline water, which may significantly overestimate CO_2 sequestration potential through solubility trapping. In order to accurately estimate CO_2 sequestration potential over geological conditions, the Peng-Robinson Cubic-Plus-Association (PR-CPA) equation of state (EOS) is used in this study to model both aqueous and nonaqueous phases. A promising flash technique at given moles, volume and temperature, known as NVT flash, is employed and the salting-out effect is reproduced by correcting the chemical potential of aqueous nonelectrolyte components. To represent real saline environments, five salts are considered,

including sodium chloride (NaCl), potassium chloride (KCl), calcium chloride ($CaCl_2$), magnesium chloride ($MgCl_2$) and sodium sulfate (Na_2SO_4). With taking into account the electrostatic contribution caused by salts, the combination of the salt-based PR-CPA EOS and NVT flash accurately models the solubility behavior of CO_2 in mixed-salt solutions and the numerical results agree with experimental data very well. Moreover, the proposed CPA model exhibits neck-to-neck accuracy to the more sophisticated electrolyte CPA EOS, thus making it promising to accurately estimate carbon sequestration potential in saline aquifers through solubility trapping.

Keywords:

CO_2 sequestration, Saline water, Thermodynamic modeling, NVT flash, Cubic-Plus-Association equation of state

1. Introduction

Nowadays, among various environmental problems, global warming is an extensively concerned issue, since the anthropogenic emission of CO_2 is imperiling the earth ecosystem and will threaten human civilization if not controlled in time. It has been reported that the Paris Agreement climate goals are being challenged due to committed emissions from existing energy infrastructure [1]. Unfortunately, fossil fuels are still believed to occupy the dominant position of the world's energy supply in the foreseeable

*Corresponding author: Shuyu Sun.

Email addresses: yiteng.li@kaust.edu.sa (Yiteng Li), zhonghua.qiao@polyu.edu.hk (Zhonghua Qiao), shuyu.sun@kaust.edu.sa (Shuyu Sun), tao.zhang.1@kaust.edu.sa (Tao Zhang)

future, due to their inherent advantages, such as large reserves, competitive cost and easy storage and transportation [2, 3]. It is imperative to find an immediately available and technologically feasible approach to reduce enormous CO_2 emissions from fossil fuel combustion, thus giving birth to the idea of CO_2 sequestration.

One economic disposal approach is injecting CO_2 into oil reservoirs to enhance oil recovery (EOR) and meanwhile sequesters CO_2 underground [4–6]. When CO_2 contacts with oil, hydrocarbon components are extracted into the less viscous CO_2 phase and, on the other hand, the dissolved CO_2 makes oil swelling so that oil can be displaced more easily [7, 8]. However, since a considerable amount of CO_2 is "lost" to the oil phase for recovery enhancement, the carbon sequestration potential in this EOR process is less than expectation. Another promising geological site for CO_2 sequestration is deep saline aquifers, which provide substantial storage capacity due to its large pore volume and wide distribution [2, 9, 10]. Most of the injected CO_2 is trapped in saline water by dissolution and such a mechanism is called solubility trapping [11, 12]. However, saline water usually has a considerable salt content and the presence of salts could significantly reduce CO_2 solubility, which is known as the salting-out effect.

Clearly, a better understanding of CO_2 solubility in saline water plays a critical role in the success of CO_2 sequestration projects [13–15]. Such a knowledge is important to design CO_2 flooding [16–19] as well since water is injected either alternately or simultaneously with the CO_2 slug [20]. More-

over, unlike other gases, the dissolution of CO_2 into aqueous phase often causes a density increase, which can induce natural convection and facilitate CO_2 mixing with water [10, 21, 22]. Therefore, it is necessary to accurately describe the aqueous-phase density when modeling CO_2 sequestration and migration in saline aquifers, making the fugacity-fugacity (ϕ-ϕ) model advantageous over the fugacity-activity (γ-ϕ) model even though the latter has been successfully applied to estimate CO_2 solubility in water/brine [23–27]. Another distinct advantage of the ϕ-ϕ approach is all fluid phases can be modeled by a single consistent equation of state (EOS) [28–31]. Popular cubic EOSs, such as Peng-Robinson (PR) EOS [32] and Soave-Redlich-Kwong (SRK) EOS [33], were used to deal with gas-water or gas-brine equilibria in combination with complicated mixing rules, improved α-term or non-symmetric binary interaction coefficients (BICs) [34–38], but these semiempirical cubic EOSs were originally designed for hydrocarbons only. As a result, they are essentially inapplicable to associating and highly polar fluids [39], e.g. water, which exhibits unusual thermodynamic behaviors due to strong hydrogen bonding interactions. There is also evidence that CO_2 can form weak hydrogen bonds in the presence of associating species [40]. As can be seen, such behaviors cannot be easily captured by conventional thermodynamic models that only take into account the physical interactions between molecules.

The establishment of Wertheim's thermodynamic perturbation theory [41] contributes to CPA EOS [42], which explicitly accounts for hydrogen

bonding interactions and takes advantage of a cubic EOS to describe physical interactions. Despite of its simple physical term, CPA EOS exhibits high computational efficiency and accuracy so that it has been extensively applied to various phase equilibria problems. During the past decade, numerous efforts have been made to accurately estimate CO_2 solubility by CPA-type models either in fresh water [43–48] or NaCl solution [49–51], both of which are far from the composition of real saline environments. In reality, saline water consists of a varity of salts, including NaCl, KCl, $CaCl_2$, $MgCl_2$, Na_2SO_4, etc. Unfortunately, no representative salinity composition has been reported so far since it is highly dependent on the local geological condition of saline water. Despite this, the salting-out effect of different salts cannot be fully represented by a single salt. Thus, accurate evaluation of CO_2 sequestration potential heavily relies on modeling of CO_2 solubility behavior in mixed-salt solutions. Just recently, Sun et al. [52] applied their electrolyte CPA EOS, also called e-CPA EOS, to estimate CO_2 solubility in both single- and mixed-salt solutions. The electrostatic contributions in their model has two sources, the ion-ion long range interactions described by the Debye-Hückel (DH) theory and the solvation interactions represented by the Born term. By tuning ion-based parameters to the experimental data, they successfully modeled CO_2 solubility behaviors in single- and mixed-salt solutions, which exhibited satisfactory agreement with experimental data.

Despite the fact that most of CPA models use SRK EOS as the physical term, recently PR-CPA (Peng-Robinson Cubic-Plus-Association) EOS

has gained popularity and achieved great success in various engineering problems, such as inhibition of gas hydrate formation [53], removal of acid gas [54, 55], as well as production of bitumen [56]. However, it has not been extended to phase behavior modeling of CO_2-brine systems. Thus, in this study, PR-CPA EOS is used to estimate CO_2 solubility in mixed-salt solutions, which comprise the five salts mentioned above. The salting-out effect is reproduced by correcting the chemical potential of aqueous nonelectrolyte components. More importantly, the distinct difference between this work and all the other works is phase equilibria modeling is performed at given moles, volume and temperature (the so-called NVT flash), instead of the conventional NPT flash framework. The new variable specification exhibits inherent advantages, such as well-posed formulation, unique pressure-volume relation, as well as promising potential in compositional flow simulation [57]. The NVT flash also has appealing properties for both implicit flow simulation [58] and semi-implicit flow simulation [59, 60]. Numerous efforts have been made to enhance computational performance of NVT flash calculations [61–66] and extend its applications [67–72]. It is worth mentioning that Jindrová and Mikyška [73] previously modeled phase equilibria of CO_2-H_2O mixture under the NVT flash framework with their PR-CPA EOS to estimate the potential of CO_2 sequestration. However, they neither considered the effect of salts nor compare their results with experimental data. To the best of our knowledge, this is the first time that the combination of NVT flash and salt-based PR-CPA EOS is applied to deal with

phase equilibria for CO_2-brine systems over geological storage conditions. Numerical results demonstrate that the proposed therymodynamic model can accurately estimate CO_2 solubility in saline water and it exhibits neck-to-neck accuracy in comparison to the more sophisticated e-CPA model proposed by Sun et al. [52].

The remainder of this paper is organized as follows. In the following section, we first formulate the NVT flash problem to model two-phase equilibrium between CO_2 and brines. Next, data and parameter optimization are elaborated. In Section 4, we present numerical results for single- and mixed-salt solutions and discuss the results. At the end, we make our conclusions in Section 5.

2. Thermodynamic modeling

2.1. Phase equilibria between CO_2 and H_2O

PR-CPA EOS takes advantage of PR EOS to describe the physical interactions between CO_2 and H_2O while the thermodynamic perturbation theory models associating interactions. Thus, the Helmholtz free energy density $f(\boldsymbol{n})$ has two components

$$f(\boldsymbol{n}) = \frac{F(\boldsymbol{n})}{V} = f^{\mathrm{PR}}(\boldsymbol{n}) + f^{\mathrm{assoc}}(\boldsymbol{n}) \tag{1}$$

where F is Helmholtz free energy, V is the volume of fluid mixture and $\boldsymbol{n}$ is the vector of molar concentrations. The physical contribution f^{PR} is formulated based on PR EOS

$$f^{\mathrm{PR}} = RT \sum_i n_i \left(\ln n_i - 1\right) - nRT \ln\left(1 - bn\right) + \frac{a(T)n}{2\sqrt{2}b} \ln\left(\frac{1 + (1 - \sqrt{2})bn}{1 + (1 + \sqrt{2})bn}\right), \tag{2}$$

where R is the universal gas constant, T is the temperature, $n = \sum_i n_i$ is the overall molar concentration. $a(T)$ and b represent the energy and co-volume parameter of the fluid mixture, which can be computed by the classical Van der Waals mixing rule

$$a(T) = \sum_i \sum_j x_i x_j \left(a_i a_j\right)^{1/2} \left(1 - k_{ij}\right) , \quad b = \sum_i x_i b_i , \tag{3}$$

where $a_i = a_i^0 \left[1 + c_i \left(1 - \sqrt{T/T_{c,i}}\right)\right]^2$, x_i is the mole fraction of component i, and k_{ij} is the BIC between component i and j. For nonwater species,

$$a_i^0 = 0.45724 \frac{R^2 T_{c,i}^2}{P_{c,i}} , \tag{4}$$

$$b_i = 0.07780 \frac{R T_{c,i}}{P_{c,i}}, \tag{5}$$

$$c_i = \begin{cases} 0.37464 + 1.54226\omega_i - 0.26992\omega_i^2 , & \text{if } \omega_i < 0.5 \\ 0.3796 + 1.485\omega_i - 0.1644\omega_i^2 + 0.01667\omega_i^3 , & \text{if } \omega_i \geq 0.5 \end{cases} \tag{6}$$

where $P_{c,i}$, $T_{c,i}$ and ω_i denote the critical pressure, critical temperature and acentric factor of component i, respectively.

According to the Wertheim's perturbation theory, the association contribution to Helmholtz free energy density is given by

$$f^{\text{assoc}} = RT \sum_i n_i \sum_{A_i} \left(\ln X_{A_i} - \frac{1}{2} X_{A_i} + \frac{1}{2}\right) , \tag{7}$$

where X_{A_i} is the unbonded site fraction of site A on component i, which can be solved from the following nonlinear equation system

$$X_{A_i} = \frac{1}{1 + \sum_j n_j \sum_{B_j} X_{B_j} \Delta^{A_i B_j}} \,, \tag{8}$$

with association strength

$$\Delta^{A_i B_j} = g \beta^{A_i B_j} \left[\exp\left(\frac{\varepsilon^{A_i B_j}}{RT} \right) - 1 \right] b_{ij} \,. \tag{9}$$

In Eq. (9), $\beta^{A_i B_j}$ and $\varepsilon^{A_i B_j}$ are the association volume and association energy parameter between site A on component i and site B on component j. $b_{ij} = (b_i + b_j)/2$ is the cross co-volume parameter. The radial distribution function is approximated by $g = 1/(1 - 1.9\eta)$ [74], where $\eta = bn/4$ is the reduced density. Clearly, it is not straightforward to directly solve X_{A_i} from Eq. (8). Instead, the iterative algorithm proposed by Michelsen [75] is employed here to efficiently compute X_{A_i} with no worry about the association scheme of CO_2 and H_2O molecules.

Similarly, chemical potential and pressure consist of both physical and association components as well

$$\begin{aligned} \mu_i &= \mu_i^{\mathrm{PR}} + \mu_i^{\mathrm{assoc}} + \Delta\mu_i^{\mathrm{DH}} \,, \\ P &= P^{\mathrm{PR}} + P^{\mathrm{assoc}} \,. \end{aligned} \tag{10}$$

In addition, the expression of chemical potential includes an additional contribution in the presence of salts, which is denoted as $\Delta\mu_i^{\mathrm{DH}}$. For the CO_2-H_2O system, $\Delta\mu_i^{\mathrm{DH}} = 0$. Details on modeling of $\Delta\mu_i^{\mathrm{DH}}$ will be described in subsection 2.2. The physical contributions to chemical potential and pressure are

$$\mu_i^{\mathrm{PR}} = RT\ln n_i - RT\left(\ln\left(1-bn\right) - \frac{nb_i}{1-bn}\right) + \frac{2\left(\sum_{j=1}^{M} x_j a_{ij}\right) b - ab_i}{2\sqrt{2}b^2}\times \ln\left(\frac{1+(1-\sqrt{2})bn}{1+(1+\sqrt{2})bn}\right) + \frac{a(T)n}{2\sqrt{2}b}\left(\frac{(1-\sqrt{2})b_i}{1+(1-\sqrt{2})bn} - \frac{(1+\sqrt{2})b_i}{1+(1+\sqrt{2})bn}\right), \tag{11}$$

$$P^{\mathrm{PR}} = \frac{nRT}{1-bn} - \frac{a(T)n^2}{1+2bn-(bn)^2}, \tag{12}$$

where $a_{ij} = (a_i a_j)^{1/2}(1-k_{ij})$. On the other hand, the association contributions can be computed by taking advantage of the stationary point of the well-defined Q function in [76], which yields

$$\mu_i^{\mathrm{assoc}} = RT\left[\sum_{A_i}\ln X_{A_i} - \frac{1}{2}\sum_{i=1}^{M} n_i \sum_{A_i}\left(1-X_{A_i}\right)\frac{\partial \ln g}{\partial n_i}\right], \tag{13}$$

$$P^{\mathrm{assoc}} = -\frac{1}{2}RT\left(1+\eta\frac{\partial \ln g}{\partial \eta}\right)\sum_{i=1}^{M} n_i \sum_{A_i}\left(1-X_{A_i}\right). \tag{14}$$

Note that the NVT flash requires the chemical equilibrium condition ($\mu_i^{\mathrm{naq}} = \mu_i^{\mathrm{aq}}$) and mechanical equilibrium condition ($P^{\mathrm{naq}} = P^{\mathrm{aq}}$) are simultaneously satisfied at the equilibrium state. The superscript naq and aq represent the nonaqueous and aqueous phase. Chemical potential and pressure in each phase can be calculated from Eq. (10) to (14).

2.2. Modeling of electrolyte solutions

Real formation water or saline water usually has a considerable salt content and could significantly inhibit the dissolution of CO_2 in water, which is known as the salting-out effect. Thus, it is of vital importance to take into account the effect of salts on phase equilibria modeling of CO_2-brine systems. In this study, we assume salts only exist in the aqueous phase.

The chemical potential of each nonelectrolyte component in the aqueous phase is corrected by introducing the DH activity coefficient [77]

$$\ln \gamma_i^{\mathrm{DH}} = \frac{2AM_m h_{is}}{B^3} f(BI^{\frac{1}{2}}) \,, \tag{15}$$

with

$$f(BI^{\frac{1}{2}}) = 1 + BI^{\frac{1}{2}} - \frac{1}{\left(1 + BI^{\frac{1}{2}}\right)} - 2\ln\left(1 + BI^{\frac{1}{2}}\right) \,, \tag{16}$$

where M_m is the molecular weight of salt-free mixture, h_{is} is the interaction parameter between nonelectrolyte component and salt, and the ionic strength

$$I = \frac{1}{2}\sum_j m_j z_j^2 \,, \tag{17}$$

where m_j and z_j is the molality and ionic charge of ion j for a given salt, respectively. The coefficient A and B in Eq. (15) have the following form

$$A = 1.327757 \times 10^5 \frac{{\rho_m}^{\frac{1}{2}}}{(\eta_m T)^{\frac{3}{2}}} \,, \quad B = 6.35969 \frac{{\rho_m}^{\frac{1}{2}}}{(\eta_m T)^{\frac{1}{2}}} \,, \tag{18}$$

where ρ_m is the mass density, $\eta_m = x_w \eta_w$ is the dielectric constant of the salt-free mixture, x_w is the mole fraction of water and η_w is the dielectric constant of pure water at given density and temperature.

It can be seen from Eq (15) that the interaction parameter h_{is} plays a critical role in accurate modeling of CO_2 solubility in brines. In particular, the interaction parameter h_{ws}, between water and salts, is considered as a function of salt concentration and temperature [78]

$$h_{ws} = \frac{A_{ws}}{W} + B_{ws}W^2 + \frac{C_{ws}}{W^2} + D_{ws} + E_{ws}(T - 273.15) \,, \tag{19}$$

while the interaction parameter between CO_2 and salts, h_{cs}, is assumed to

depend on temperature only [79],

$$h_{cs} = A_{cs}T^2 + B_{cs}T + C_{cs}\,, \tag{20}$$

where W is salt concentration in weight percent and T is temperature in Kelvin. Since the excess chemical potential follows $\mu_i^E = RT\ln\gamma_i$, the DH electrostatic contribution to chemical potential can be modeled by $\Delta\mu_i^{\mathrm{DH}} = RT\ln\gamma_i^{\mathrm{DH}}$. For a mixed-salt solution, the overall electrostatic contribution to chemical potential of a nonelectrolyte component is modeled based on the relationship proposed by [80]

$$\Delta\mu_i = \sum_{j=1}^{N_s} w_j \Delta\mu_{i,j}^0\,, \quad w_j = \frac{I_j}{\sum_j I_j} \tag{21}$$

where N_s is the number of salts, w_j is the ionic strength fraction of salt j, and $\mu_{i,j}^0$ is the chemical potential of component i in the single-salt solution j at the overall ionic strength.

Similar to confined phase equilibria problems that take into account capillary effect, the additional chemical potential contribution converts the original optimization problem into an equation-solving problem [66] where the symmetric Jacobian matrix, commonly used to design efficient numerical algorithm, no longer exists. To enhance the convergence performance, a VT-based successive substitution iteration (SSI) [66, 81] is used to initialize Newton iterations. Moreover, the two-stage line search scheme is applied to ensure the computed variables sit inside their physically meaningful ranges and Helmholtz free energy constantly dissipates over iterations. If energy dissipation stops before it reaches the stopping criterion, we switch back to

SSI and continue phase equilibria calculation at the given condition. It is also worth mentioning that CPA EOS has a near-cubic behavior [42]. In other words, typically there are three real roots when solving the volume equation under the NPT flash framework. As a result, root selection has to be performed in certain rules, which may result into slow convergence or even incorrect solution for NPT flash if roots are improperly selected at the early stage. In contrast, this can be avoided in NVT flash calculation since each pressure corresponds to a unique volume.

3. Parameter optimization

To accurately model phase behavior using the CPA-type EOS, it is crucial to optimize parameters by fitting the experimental data. Moreover, the success of any association model depends on the association scheme and association approach of the investigated molecules, which could heavily affect the fitted parameters. A large amount of literature investigated which combination of association scheme and approach works best for the CO_2-H_2O system. Unfortunately, the optimal combination remains unclear [82]. In this study, both H_2O and CO_2 are assumed as 4-site molecules with two proton donors and two proton acceptors. Such association schemes have been extensively used in the literature. We consider CO_2 as a solvating molecule, which is only allowed to cross associate with H_2O. In the rest of this section, the shuffled complex evolution method proposed by Duan et al. [83] is used for parameter optimization. In addition, instead of using the sum of squared errors as the objective function, the absolute average

deviation (AAD), often used to indicate fitting errors, is directly minimized in our fitting process, which could help us avoid overfitting those outliers that are incorrectly or improperly measured in experiments [82]

$$\mathrm{AAD}\% = \frac{1}{N_p}\sum_{i=1}^{N_p}\left|\frac{x_i^{\mathrm{cal}} - x_i^{\mathrm{exp}}}{x_i^{\mathrm{exp}}}\right| \times 100\,, \tag{22}$$

where N_p is the number of data points, x_i^{cal} and x_i^{exp} represent the computed result and experiment data of the given property, respectively.

3.1. Physical and association parameters for water

To reproduce phase behavior of H_2O, all five pure-compound parameters, including a_i^0, b_i, c_i, $\varepsilon^{A_iB_j}$ and $\beta^{A_iB_j}$, are tuned by fitting experimental data of saturated vapor pressure and liquid density [84, 85], obtained from DIPPR database. The fitting process is performed over the temperature range $0.42 < T_{r,w} < 0.95$, where $T_{r,w}$ denotes the reduced temperature of water. Figure 1 compares the computed vapor pressure and liquid density using the optimized parameters with the experiment data. It can be seen the computed saturation pressures agree with the measurements very well but the computed liquid density is slightly overestimated at low temperature. On the other hand, since saturation vapor pressures and liquid densities of CO_2 can be accurately estimated using the critical pressure, temperature and acentric factor (shown in Table 1), it is decided to use Eq. (4), (5) and (6) to compute a_i^0, b_i and c_i rather than re-estimate these parameters for CO_2. In addition, thanks to the introduction of the cross association factor, it is unnecessary to parameterize $\varepsilon^{A_iB_j}$ and $\beta^{A_iB_j}$ for CO_2. Table 2 shows

the pure-compound parameters of H_2O and CO_2 and the corresponding AAD of saturated vapor pressure and liquid density.

Table 1: Compositional properties of H_2O and CO_2.

Component	$T_{c,i}$ [K]	$P_{c,i}$ [Pa]	ω_i	$M_{w,i}$ [kg · mol^{-1}]
H_2O	647.29	2.209×10^7	0.3440	0.01802
CO_2	304.14	7.375×10^6	0.2390	0.04401

Table 2: Physical and association parameters of H_2O and CO_2.

Component	a_0 [Pa · (m^3/mol)^2]	b [m^3/mol]	c_1	ε [Pa · m^3/mol]	β	AAD %	
						P_{vapor}	ρ_{liquid}
H_2O	0.1405	1.4759×10^{-5}	1.2088	1.4159×10^4	0.1134	0.20	1.06
CO_2	0.3962	2.6652×10^{-5}	0.7060	-	-	0.78	2.55

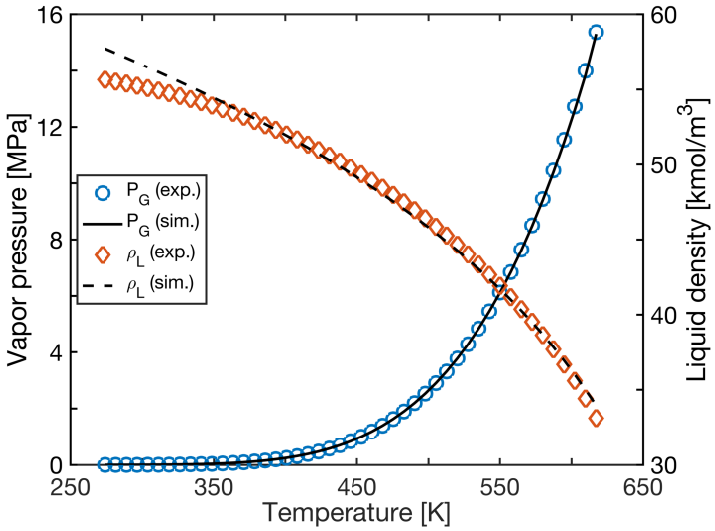

Figure 1: Fitting experimental vapor pressure and liquid density data for H_2O. The experimental data are obtained from DIPPR database.

3.2. Binary interaction coefficient and cross-association factor

Another two important parameters for phase equilibria modeling of CO_2-H_2O system are BIC, k_{ij}, and the cross association factor, s_{ij}, which describes the cross-association strength between CO_2 and H_2O. Essentially, tuning the cross-association factor is equivalent to tuning the cross-association volume in the modified CR-1 combining rule proposed by Folas et al. [86]. The cross-association strength is computed by the product of self-association strength of H_2O and s_{ij} [87]. To better represent k_{ij} and s_{ij}, most literature considers they are strongly temperature-dependent. By extensively testing the performance of published expressions, we adopt $k_{ij} = a_1 T_{r,\mathrm{CO_2}} + a_2$ where $T_{r,\mathrm{CO_2}}$ denote the reduced temperature of CO_2, and $s_{ij} = b_1 T_{r,\mathrm{CO_2}}^3 + b_2 T_{r,\mathrm{CO_2}}^2 + b_3 T_{r,\mathrm{CO_2}} + b_4$. Six coefficients a_1, a_2, b_1, b_2, b_3 and b_4 are fitted to the experimental solubility data of CO_2-H_2O mixtures. In order to obtain the most accurate and reliable data, Aasen et al. [82] conducted an exhaustive literature review to evaluate published experimental data. Here we use all the available data that we can ensure their accuracy and reliability from the suggested publications [37, 46, 88–96] to tune the six coefficients mentioned above, which yields

$$k_{ij} = 0.6546 T_{r,\mathrm{CO_2}} - 0.6165\,, \tag{23}$$

$$s_{ij} = -0.4254 T_{r,\mathrm{CO_2}}^3 + 1.6922 T_{r,\mathrm{CO_2}}^2 - 1.9815 T_{r,\mathrm{CO_2}} + 0.7380\,, \tag{24}$$

with the AAD of 4.91 % for CO_2 solubility in the H_2O-rich phase and AAD of 9.79 % for H_2O solubility in the CO_2-rich phase. Figure 2 shows the

values of k_{ij} and s_{ij} over the temperature range $T \in [278, 478]$ K.

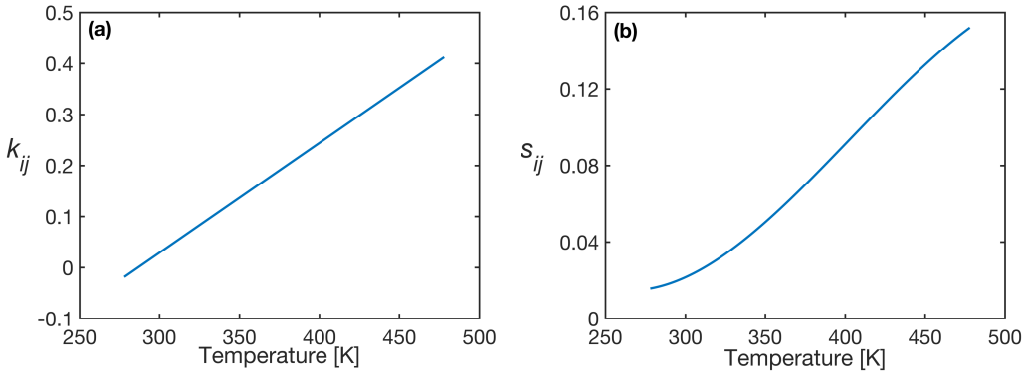

Figure 2: Binary interaction coefficient k_{ij} (a) and cross-association factor s_{ij} (b) as a function of temperature at $T \in [278, 478]$ K for CO_2-H_2O system.

3.3. Interaction paramters between nonelectrolyte component and salt

Accurate description of CO_2 solubility behavior in saline water places importance on the optimization of the H_2O-salt interaction parameter, h_{ws}, and CO_2-salt interaction parameter, h_{cs}. For this purpose, the five coefficients in h_{ws}, see Eq. (19), are fitted to the experimental freezing point depression data by modeling phase equilibria between the aqueous single-salt solution and its ice phase at the ice vapor pressure. We collect all the available experimental data for NaCl [78, 97–101], KCl [97, 99, 101], $CaCl_2$ [78, 97, 100–103], $MgCl_2$ [78, 97, 98, 101, 102, 104] and Na_2SO_4 [101, 104, 105] from the publications suggested in [78]. The optimized coefficients of h_{ws} are shown in Table 3. Figure 3 displays the computed melting temperatures together with the experimental data. It can be seen the fitted coefficients accurately predict the melting temperature of each single-salt so-

lution as the salt concentration increases. In addition, the three coefficients in h_{cs}, see Eq. (20), are optimized using the experimental solubility data of CO_2 in the NaCl [93, 106–109], KCl [110–112], $CaCl_2$ [112–114] $MgCl_2$ [112, 114], and Na_2SO_4 [112, 115] solution, respectively. Table 4 shows the investigated temperature and molality ranges where the coefficients of h_{cs} are applicable and the AAD of CO_2 solubility in each single-salt solution. Overall, the optimized coefficients yield satisfactory accuracy, of which the CO_2-$CaCl_2$ interaction parameter exhibits a little higher AAD than others.

Table 3: Optimized coefficients for the H_2O-salt interaction parameter h_{ws}.

	A	B	C	D	E/K	AAD %
NaCl	−9.4875	−0.0011	−0.1569	−7.7593	0.1998	0.011
KCl	−11.7708	−0.0018	−0.0336	−7.8928	0.0495	0.010
$CaCl_2$	−2.1142	−0.0035	−0.0380	−4.3097	0.1768	0.036
$MgCl_2$	−1.7205	−0.0173	−0.0499	−4.7829	0.0100	0.040
Na_2SO_4	−7.6939	−0.0014	−0.0074	−2.3803	0.0067	0.036

Table 4: Optimized coefficients for the CO_2-salt interaction parameter h_{cs}.

	T [K]	M [mol/kg]	A $\times 10^{-5}$	B	C	AAD %
NaCl	293.08 - 433.08	0.25 - 6.00	−1.9837	−0.1334	85.2549	4.26
KCl	313.1 - 433.1	0.50 - 4.50	1.3679	−0.0236	26.1853	4.72
$CaCl_2$	298.15 - 424.64	0.18 - 5.00	−21.475	0.0872	27.7695	5.81
$MgCl_2$	309.52-424.68	0.333 - 5.00	59.180	−0.4799	125.4637	4.70
Na_2SO_4	286.97 - 423	0.25 - 2.00	0	−0.2498	130.3604	4.54

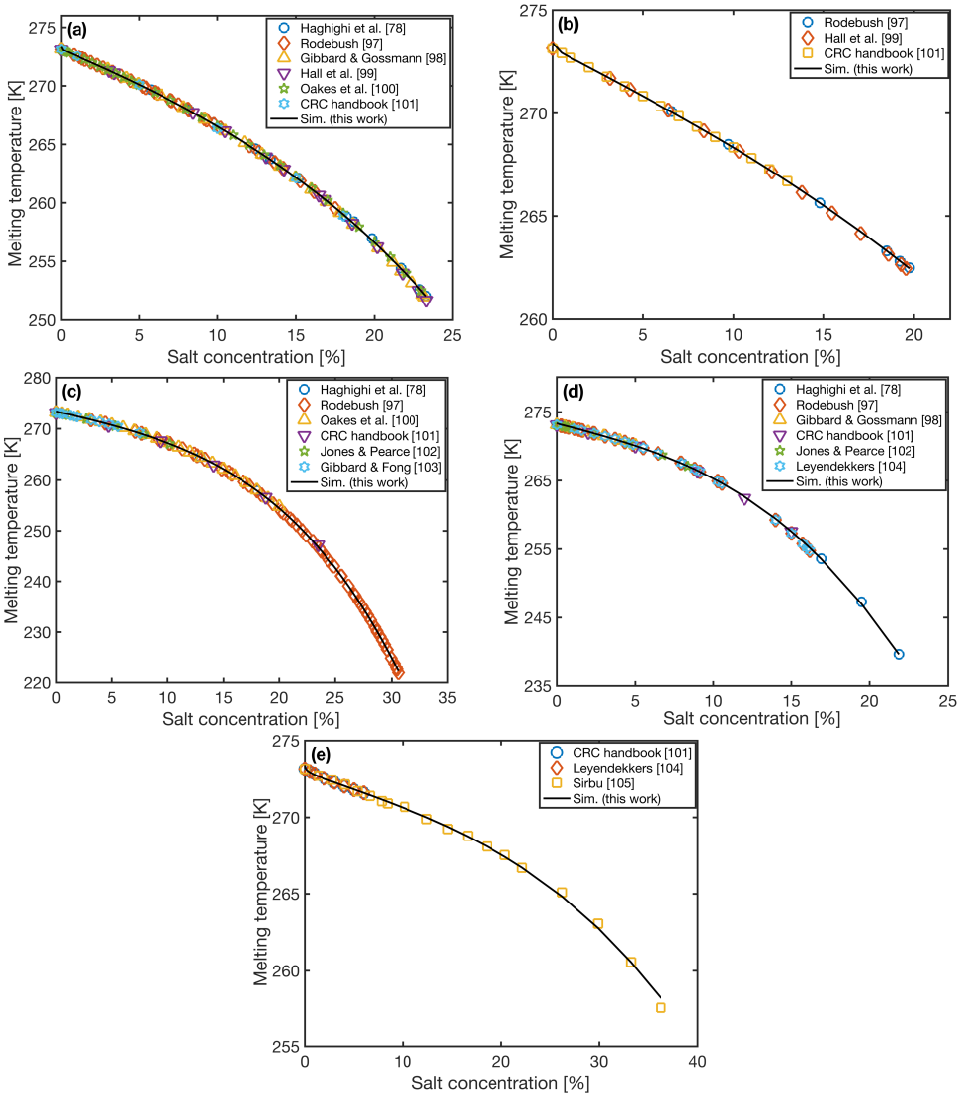

Figure 3: Fitting experimental freezing point depression data of single-salt solutions: (a) NaCl [78, 97–101]; (b) KCl [97, 99, 101]; (c) $CaCl_2$ [78, 97, 100–103]; (d) $MgCl_2$ [78, 97, 98, 101, 102, 104]; (e) Na_2SO_4 [101, 104, 105].

4. Results and discussion

4.1. Model validation

To validate the proposed model, we first compare the computed CO_2 solubility in single-salt solutions with experimental data. Figure 4 shows the mole fraction of CO_2 dissolved in NaCl solution at $T = 323$ K. The circle, diamond and square symbol represents measured CO_2 solubility data in the NaCl solution with molality of 1, 3 and 5 mol/kg water, respectively. It can be seen the computed results agree with the experimental data very well, while the CO_2 solubility is slightly overestimated in the NaCl solution of 1mol/kg water when pressure is greater than 20 MPa. Moreover, we compare our results with Sun et al. [52]'s results, which are shown as dash lines in the following figures. As can be seen, their electrolyte CPA model estimates CO_2 solubility at low salt molality (1 mol/kg water) better than ours, but it overestimates CO_2 solubility a little at high salt molality (5 mol/kg water). Both models exhibit the salting-out effect becomes more significant as the salt concentration increases.

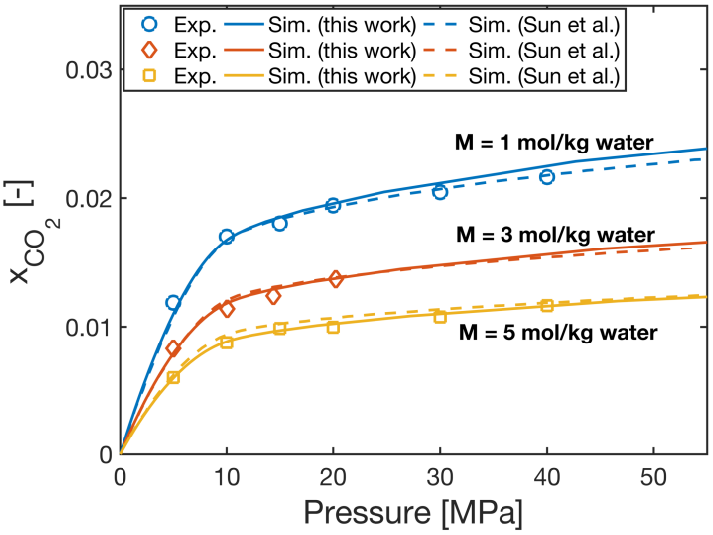

Figure 4: CO_2 solubility in the NaCl solution at $T = 323$ K with molality of 1 mol/kg (blue) , 3 mol/kg (red) and 5 mol/kg (yellow) water, respectively. The experimental data are obtained from [93] and [107].

Figure 5 displays the computed CO_2 solubility in the $CaCl_2$ solutions of 1.01 and 2.28 mol/kg water together with experimental data. At lower molality, Sun et al. [52] e-CPA EOS slightly outperforms the proposed model at $T = 349$ K. Both models can predict CO_2 solubility behavior in the 2.28 m $CaCl_2$ solution well, although the proposed model slightly underestimates while the e-CPA model overestimates the amount of CO_2 dissolved in $CaCl_2$ solution. By plotting the computed results together, as shown in Figure 6, we find CO_2 solubility at $T = 349$ K intersects with CO_2 solubility at $T = 374$ K, which was also observed by [52]. Interestingly, at a fixed salt concentration, CO_2 solubility at $T = 374$ K is not always lower than that at $T = 349$ K, which is contradictory to the general knowledge. The salting-

out effect at $T = 374$ K gets weakened as pressure exceeds around 35 MPa, implying the high-temperature $CaCl_2$ solution could provide extra storage capacity at high pressures.

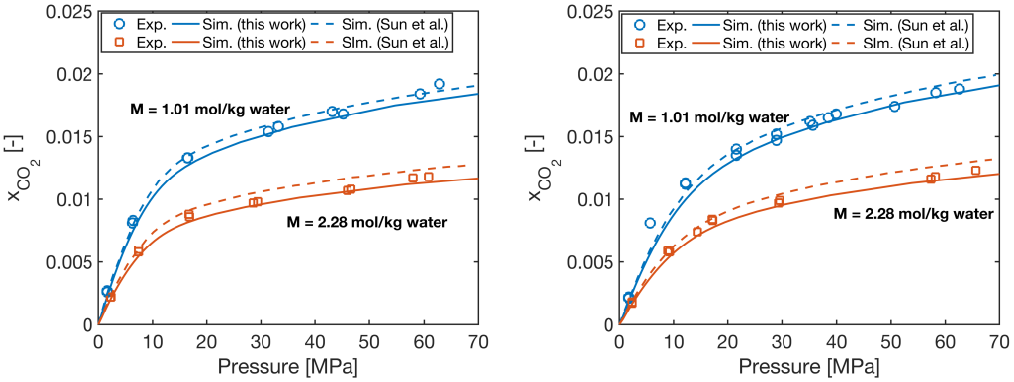

Figure 5: CO_2 solubility in the $CaCl_2$ solution at $T = 349$ K (left) and $T = 374$ K (right). All the experimental data are obtained from [113].

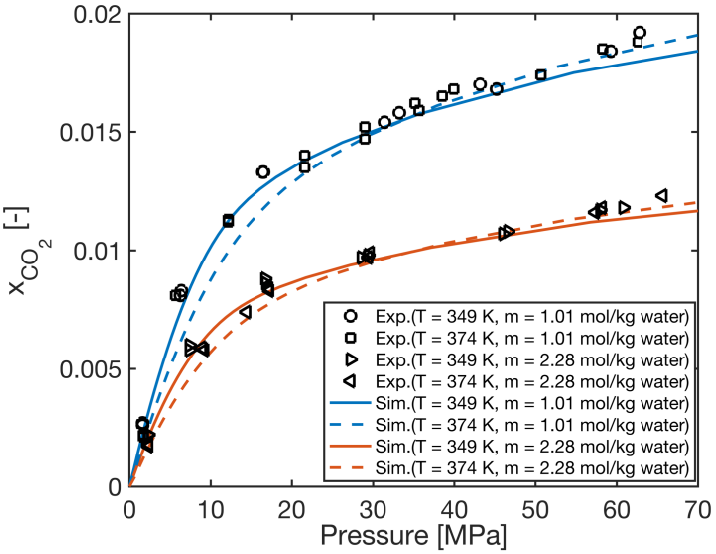

Figure 6: CO_2 solubility in the $CaCl_2$ solution. The experimental data [113] and computed results are represented by symbols and lines, respectively.

The last example for model validation compares the experimental data, obtained from [106], with computed CO_2 solubility in Na_2SO_4 solutions with molality of 1 and 2 mol/kg water at two different temperatures, as shown in Figure 7. At $T = 313$ K, the proposed CPA model has the same accuracy with the e-CPA EOS [52]. Clearly, CO_2 solubilities in two salinity solutions are underestimated, even though the e-CPA EOS accounts for the ion solvation by an additional Born term. On the other hand, the e-CPA model yields higher prediction accuracy at $T = 333$ K. Several reasons may account for the poor performance of the proposed model for Na_2SO_4 solutions. Above all, the measured CO_2 solubility data in Na_2SO_4 solutions are much less than in NaCl and $CaCl_2$ solutions. A smaller number of experimental data are used to tune the interaction parameter between CO_2 and Na_2SO_4 so that the prediction accuracy is somewhat unsatisfactory. Moreover, the fitting data used for parameter optimization in this study is partially inconsistent with the experimental data used by Sun et al. [52]. Some data in their work are unavailable for us and thereby we have to use other data as a replacement. Also, experimental measurements may have errors, which is another reason for the poor performance that cannot be ignored. It is worth mentioning that the proposed model doesn't take into account the effect of ion size on CO_2 solubility behavior, which may play an important role in Sun et al. [52]'s model to accurately estimate the amount of dissolved CO_2 in Na_2SO_4 solutions. In addition, we also compare the

estimated CO_2 solubility in 1, 2 and 3 m[1] Na_2SO_4 solutions at $T = 348$ K with the experimental data [116] in Figure 8, which are recently found and not used to tune the interaction parameter between CO_2 and Na_2SO_4. The computed results match up with the new experimental data very well. It is worth mentioning that the CO_2-Na_2SO_4 interaction parameter is tuned up to $M = 2$ mol/kg water. The yellow dash line in Figure 8 is predicted outside the molality range, see Table 4, and it shows great accuracy and consistency with the experimental data.

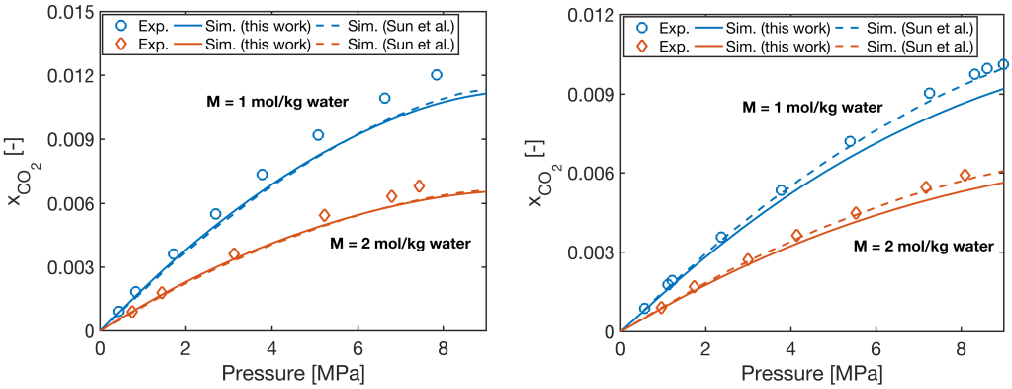

Figure 7: CO_2 solubility in the Na_2SO_4 solution at $T = 313$ K (left) and $T = 333$ K (right). Experimental data are obtained from [106].

[1]A solution with molality of X mol/kg is often denoted as X m. Here m is the abbrevitation of molality unit rather than length unit.

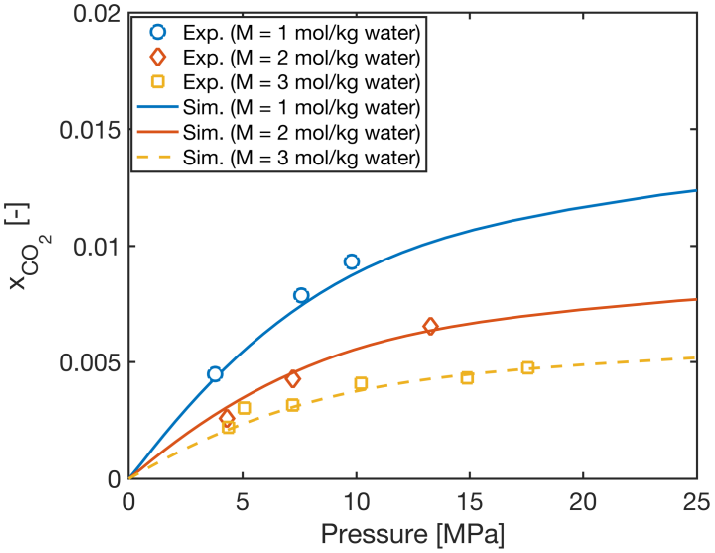

Figure 8: CO_2 solubility in the Na_2SO_4 solution at $T = 348$ K with molality of 1, 2 and 3 mol/kg water. The dash line is predicted beyond the molality range M $\in [0.25, 2.00]$ mol/kg where $h_{CO_2-Na_2SO_4}$ is tuned. All the experimental data are obtained from [116].

4.2. CO_2 solubility prediction in mixed-salt solutions

Figure 9 displays the mole fraction of CO_2 dissolved in the NaCl-KCl, NaCl-$CaCl_2$ and KCl+$CaCl_2$ solution at $T = 318$ K with the total salt concentration of 10 wt.%. The weight ratio of NaCl : KCl, NaCl : $CaCl_2$ and KCl : $CaCl_2$ is 1 : 1. Similar to the results of [52], the proposed CPA model predicts CO_2 solubility in the NaCl-$CaCl_2$ solution much better than the NaCl-KCl and KCl-$CaCl_2$ solutions. Although the experimental data [117] present that the 10 wt.% NaCl-KCl and KCl-$CaCl_2$ solutions have close salting-out effect on CO_2 solubility above 10 MPa, both models

exhibit the salting-out effect of KCl-$CaCl_2$ solution is stronger than NaCl-KCl solution, since the combination of KCl and $CaCl_2$ at the 10 wt.% salt concentration yields larger ionic strength. Overall, the prediction accuracy is still acceptable.

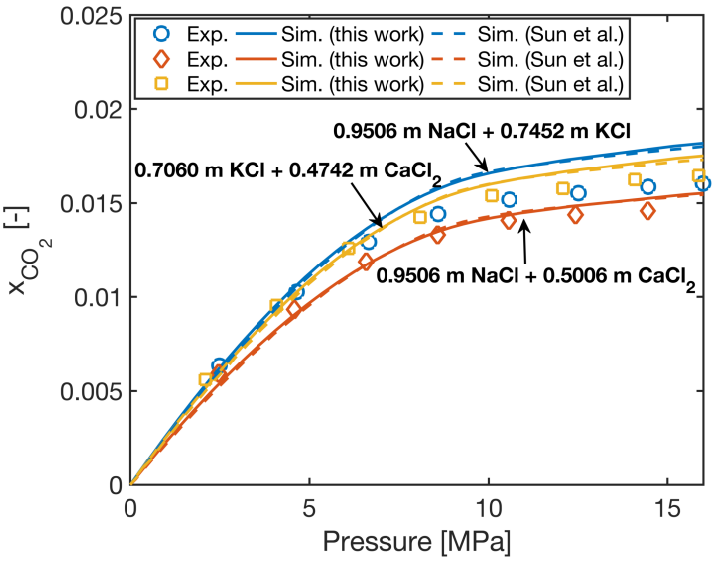

Figure 9: CO_2 solubility in the NaCl+KCl solution (blue), NaCl+$CaCl_2$ solution (red) and KCl+$CaCl_2$ solution (yellow) at $T = 318$ K with the total salt concentration of 10 wt.%. All the experimental data are obtained from [117].

The solubility behavior of CO_2 in the NaCl-KCl, NaCl-$CaCl_2$ and KCl+$CaCl_2$ solutions, shown in Figure 9, can be qualitatively explained from the perspective of kosmostrope and chaotrope. With the same anion, it mainly depends on the effect of cations on the structure of water. Overall, the presence of salt reduces CO_2 solubility in the aqueous solution since wa-

ter molecules aggregate around ions and consequently less H_2O associates with CO_2. However, a kosmotropic (structure-breaking) cation, e.g. Ca^{2+}, contributes to the stability and structure of water-water interaction, and instead, a chaotropic (structure-making) cation, e.g. K^+, disrupts the hydrogen bonding interactions between water molecules. Considering the interaction strength between CO_2 and H_2O is much weaker than the hydrogen bonding interactions between H_2O, the introduction of chaotropic ions could increase the potential of CO_2 associating with H_2O through their weak hydrogen bonding interactions. It is worth noting that Na^+ can be categorized as a borderline ion due to its neutral effect on the structure of water [118]. Thus, it is easy to find that CO_2 solubility in the NaCl-$CaCl_2$ solution should be smaller than in the NaCl-KCl at the same salt concentration. Even though the structure-making effect of Ca^{2+} could compensate for the structuring-breaking effect of K^+, the interaction strength of K^+-H_2O is stronger than that of Ca^{2+}-H_2O. With the salt content of KCl higher than $CaCl_2$, CO_2 solubility in the KCl+$CaCl_2$ solution should be smaller than NaCl-KCl solution but greater than in the NaCl-$CaCl_2$, which agree with the prediction given by both models as shown in Figure 9.

Figure 10 displays CO_2 solubility in the NaCl-KCl-$CaCl_2$ solution at $T = 308$ K with the total salt concentration of 5 wt.%, 10 wt.% and 14.3 wt.%, respectively. The weight ratio of NaCl, KCl and $CaCl_2$ is 1 : 1 : 1 and detailed molarlity compositions are shown in the figure. As the total salt concentration increases, the salting-out effect becomes more significant.

The proposed model gives the best estimation of CO_2 solubility at 5 wt.% salt concentration and it slightly underestimates the amount of dissolved CO_2 with the total salt concentration increasing. Moreover, we investigate the effect of temperature on CO_2 solubility behavior in the 10 wt.% NaCl-KCl-$CaCl_2$, shown in Figure 11. The 10 wt.% NaCl-KCl-$CaCl_2$ solution contains 0.6338 m NaCl, 0.4968 m KCl and 0.3337 m $CaCl_2$ under the identical weight ratio. The increasing temperature aggravates molecular motion, thus making it more difficult to trap CO_2 in water. As a result, the mole fraction of dissolved CO_2 continues to decrease. Even though the computed results increasingly deviate from the experimental data with an increase of temperature, the proposed model successfully capture the decreasing CO_2 solubility behavior with good accuracy.

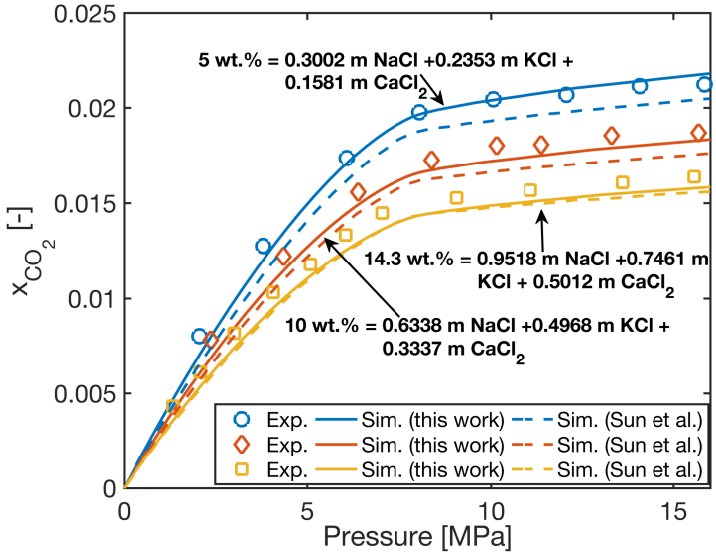

Figure 10: CO_2 solubility in $NaCl + KCl + CaCl_2$ solution with salt concentration of 5 wt.% (blue), 10 wt.% (red) and 14.3 wt.% (yellow) at $T = 308$ K. All the experimental data are obtained from [117].

In Figure 12, we compute CO_2 solubility in a quaternary-salt solution, consisting of 1.4006 m NaCl, 0.0474 m KCl, 0.3405 m $CaCl_2$ and 0.0615 m $MgCl_2$ at $T = 297$ K, and compare our results with the experimental data [119], which is an approximation of the high-salinity brine in the Appalachian Basin . The molality of each salt is close to the value used by Sun et al. [52]. Both models capture CO_2 solubility behavior in such a complex mixed-salt solution. Up to 6 MPa, the mole fraction of dissolved CO_2 increases in the $NaCl + KCl + CaCl_2 + MgCl_2$ solution and then it reaches a "plateau", indicating the sequestration potential is hardly increased any more in this saline water sample after 6 MPa.

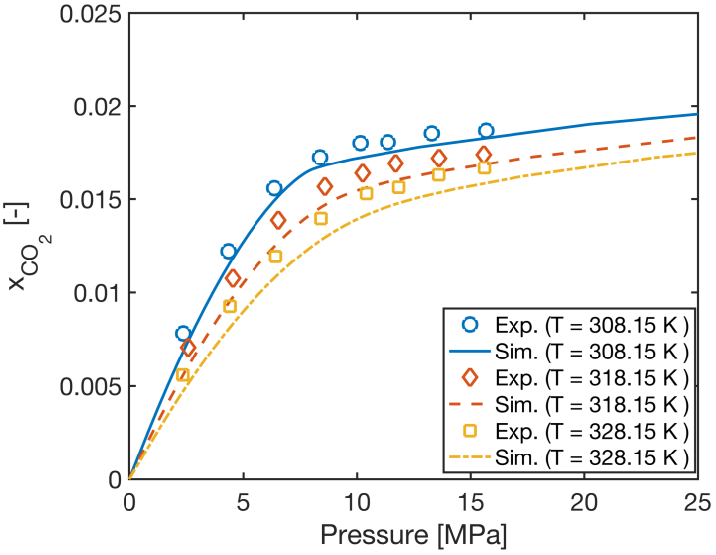

Figure 11: CO_2 solubility in $NaCl + KCl + CaCl_2$ solution of 10 wt.% salt concentration at $T = 308.15$, 318.15 and 328.15 K. All the experimental data are obtained from [117].

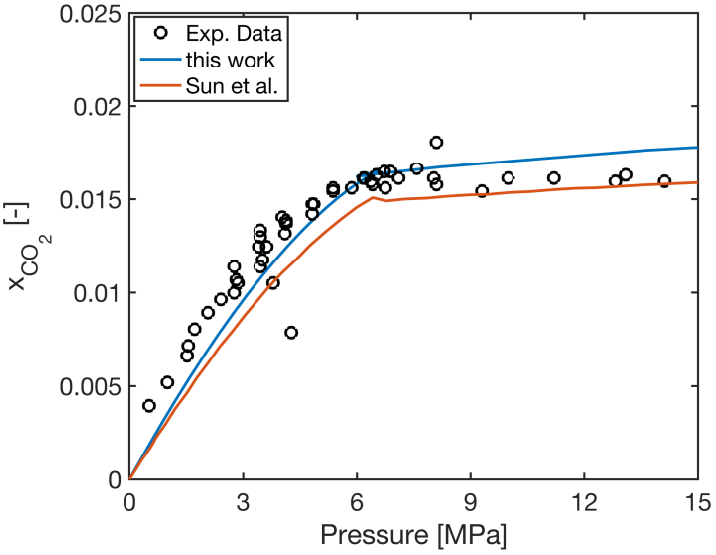

Figure 12: CO_2 solubility in mixed-salt solution consisting of 1.4006 m NaCl, 0.0474 m KCl, 0.3405 m $CaCl_2$ and 0.0615 m $MgCl_2$ at $T = 297$ K. The experimental data are obtained from [119].

At the end, the salting-out effects of all the five salts are compared. Figure 13 shows the CO_2 solubility in each single-salt solution with molality of 1 mol/kg water. The blue, red, yellow, purple and green color represents NaCl, KCl, $CaCl_2$, $MgCl_2$ and Na_2SO_4 solution respectively, and corresponding experimental data are represented by the circle [93, 107], diamond [112], square [112, 117, 120], triangle [112] and pentagram [112, 115] symbol. It can be seen the salting-out effect follows the order KCl < NaCl < $CaCl_2 \approx MgCl_2 <$ Na_2SO_4, similar to the observation of [52]. Due to the distinct salting-out effect of different salts, real saline environments cannot be fully represented by a single salt. However, a lot of literature used single

NaCl solution as a surrogate of saline water, to estimate CO_2 sequestration potential. As NaCl solution exhibits much larger solvent capacity at high pressures, this can result into overestimation of carbon sequestration potential and cause considerable economic loss due to the incorrect evaluation.

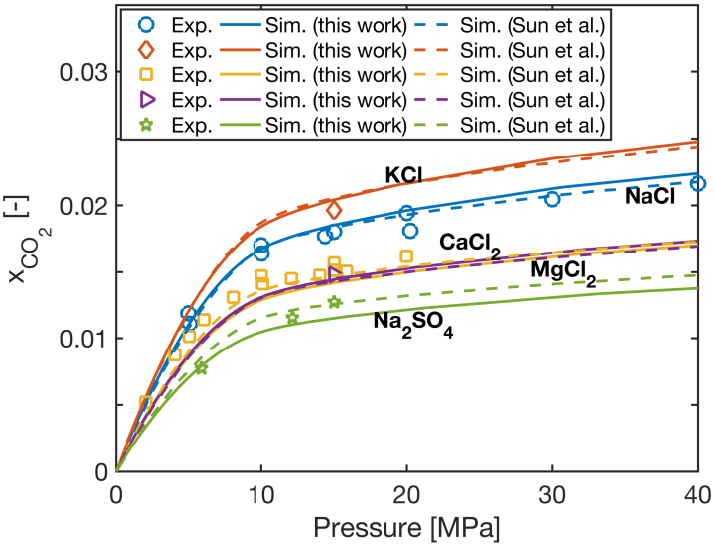

Figure 13: Comparison of CO_2 solubility in single NaCl (blue), KCl (red), $CaCl_2$ (yellow), $MgCl_2$ (purple) and Na_2SO_4 (green) solutions at $T = 323.15$ K. Each single-salt solution has molality of 1 mol/kg water.

In Figure 13, the single $CaCl_2$ solution and the $MgCl_2$ solution exhibit very close salting-out effect. However, if strictly abiding by the influence of ion charge and ion size on the salting-out effect, our results yield a little discrepancy that the salting-out effect of $CaCl_2$ is slightly stronger than that of $MgCl_2$ while the opposite is true. This may be one advantage of the electrolyte CPA EOS with ion-specific parameters. Despite this, the effect of ion charge and size is not the main focus of this work and the proposed

model gives reasonable predictions with satisfactory accuracy. If we analyze the results from the perspective of ions, or rather cations which are believed to play a dominant role in adjusting the capacity of solvent to trap dissolved gas molecules [121], it may explain why the salting-out effect follows such an order. Under the same molality, Na_2SO_4 presents the strongest salting-out effect because it has the largest cation concentration. Compared to the NaCl and KCl solution, CO_2 is less soluble in the $CaCl_2$ and $MgCl_2$ solution, implying the cation charge has a more significant impact than the cation size when comparing the salting-out effect of a divalent-cation salt with a monovalent-cation salt. Due to the larger ion size, the salting-out effect of KCl is weaker than NaCl at the same ion charge.

It can be seen the combination of NVT flash and PR-CPA EOS successfully estimate CO_2 solubility in single- and mixed-salt solutions over wide range of pressures, temperatures and salt concentrations with satisfactory accuracy. In comparison to Sun et al. [52]'s e-CPA EOS with ion-specific parameters, the PR-CPA EOS in this study may be considered as a salt-based model since interactions between nonelectrolyte component and salt are considered rather than ion and corresponding interaction parameters are tuned by fitting experimental data. Similarly, the interaction parameters of single H_2O-salt and single CO_2-salt are employed to estimate CO_2 solubility in mixed-salt solutions and no additional parameters are needed. Such a treatment significantly simplifies the complexity of phase behavior modeling of CO_2-brine systems and meanwhile preserves satisfactory accuracy.

5. Conclusions

In this study, the combination of NVT flash and PR-CPA EOS is successfully applied to model CO_2 solubility behavior in single- and mixed-salt solutions. The salting-out effect is reproduced by introducing the Debye-Hückel electrostatic contribution to chemical potential of nonelectrolyte components in the aqueous phase. Five common salts, including NaCl, KCl, $CaCl_2$, $MgCl_2$ and Na_2SO_4 are considered to represent real saline environments. To enhance the prediction accuracy, a large number of reliable experimental data are used to tune binary interaction coefficient, cross-association factor and interaction parameter between nonelectrolyte components and salts. It is shown that the combination of NVT flash and salt-based CPA model gives accurate estimation of CO_2 solubility in single- and mixed-salt solutions over wide ranges of pressure, temperature and salt concentration. More importantly, the proposed model exhibits neck-to-neck prediction accuracy with the more sophisticated e-CPA model, making it confident to accurately estimate carbon sequestration potential in saline aquifers through solubility trapping.

Acknowledgement

The authors greatly thank for the support from the National Natural Science Foundation of China (grant number 51874262, 51904031) and the Research Funding from King Abdullah University of Science and Technology (KAUST) through the grants BAS/1/1351-01, REP/1/2879-01, and

URF/1/3769-01. Z. Qiao's work is partially supported by the Hong Kong Research Council GRF grants 15300417 and 15325816 and the Hong Kong Polytechnic University fund G-UAEY.

Reference

[1] D. Tong, Q. Zhang, Y. Zheng, K. Caldeira, C. Shearer, C. Hong, Y. Qin, S. J. Davis, Committed emissions from existing energy infrastructure jeopardize 1.5°C climate target, Nature 572 (2019) 373–377. https://doi.org/10.1038/s41586-019-1364-3.

[2] S. Bachu, J. J. Adams, Sequestration of CO_2 in geological media in response to climate change: capacity of deep saline aquifers to sequester CO_2 in solution, Energy Convers. Manage. 44 (2003) 3151–3175. https://doi.org/10.1016/S0196-8904(03)00101-8.

[3] S. Chu, Carbon capture and sequestration, Science 325 (2009) 1599–1599. https://doi.org/10.1126/science.1181637.

[4] T. Holt, J. I. Jensen, E. G. B. Lindeberg, Underground storage of CO_2 in aquifers and oil reservoirs, Energy Convers. Manage. 36 (1995) 535–538. https://doi.org/10.1016/0196-8904(95)00061-H.

[5] A. G. Ravagnani, E. L. Ligero, S. B. Suslick, CO_2 sequestration through enhanced oil recovery in a mature oil field, J. Pet. Sci. Eng. 65 (2009) 129–138. https://doi.org/10.1016/j.petrol.2008.12.015.

[6] N. Mosavat, F. Torabi, Performance of secondary carbonated water injection in light oil systems, Ind. Eng. Chem. Res. 53 (2014) 1262–1273. https://doi.org/10.1021/ie402381z.

[7] M. Blunt, F. Fayers, F. M. Orr, Carbon dioxide in enhanced oil recovery, Energy Convers. Manage. 34 (1993) 1197–1204. https://doi.org/10.1016/0196-8904(93)90069-M.

[8] J. Moortgat, S. Sun, A. Firoozabadi, Compositional modeling of three-phase flow

with gravity using higher-order finite element methods, Water Resour. Res. 47 (2011) W05511. http://dx.doi.org/10.1029/2010WR009801.

[9] W. D. Gunter, S. Wong, D. Cheel, G. Sjostrom, Large CO_2 sinks: their role in the mitigation of greenhouse gases from an international, national (Canadian) and provincial (Alberta) perspective, Appl. Energy 61 (1998) 209–227. https://doi.org/10.1016/S0306-2619(98)00042-7.

[10] A. Firoozabadi, P. C. Myint, Prospects for subsurface CO_2 sequestration, AIChE J. 56 (2010) 1398–1405. https://doi.org/10.1002/aic.12287.

[11] S. M. Benson, D. R. Cole, CO2 sequestration in deep sedimentary formations, Elements 4 (2008) 325–331. https://doi.org/10.2113/gselements.4.5.325.

[12] L. X. Nghiem, V. Shrivastava, B. F. Kohse, M. S. Hassam, C. Yang, Simulation of trapping processes for CO2 storage in saline aquifers, in: Canadian International Petroleum Conference, 2009. https://doi.org/10.2118/2009-156.

[13] A. Kumar, M. H. Noh, R. C. Ozah, G. A. Pope, S. L. Bryant, K. Sepehrnoori, L. W. Lake, Reservoir simulation of CO_2 storage in aquifers, SPE J. 10 (2005) 336–348. https://doi.org/10.2118/89343-PA.

[14] T. Suekane, T. Nobuso, S. Hirai, M. Kiyota, Geological storage of carbon dioxide by residual gas and solubility trapping, Int. J. Greenhouse Gas Control 2 (2008) 58–64. https://doi.org/10.1016/S1750-5836(07)00096-5.

[15] N. I. Diamantonis, G. C. Boulougouris, D. M. Tsangaris, M. J. E. Kadi, H. Saadawi, S. Negahban, I. G. Economou, Thermodynamic and transport property models for carbon capture and sequestration (CCS) processes with emphasis on CO_2 transport, Chem. Eng. Res. Des. 91 (2013) 1793–1806. https://doi.org/10.1016/j.cherd.2013.06.017.

[16] M. John, Compositional modeling of CO2 flooding and the effect of CO2 water solubility (1982).

[17] F. M. Orr, J. P. Heller, J. J. Taber, Carbon dioxide flooding for enhanced oil recovery: Promise and problems, J. Am. Oil Chem. Soc. 59 (1982) 810A–817A.

https://doi.org/10.1007/BF02634446.

[18] Y.-K. Li, L. X. Nghiem, Phase equilibria of oil, gas and water/brine mixtures from a cubic equation of state and Henry's law, Can. J. Chem. Eng. 64 (1986) 486–496. https://doi.org/10.1002/cjce.5450640319.

[19] N. Mosavat, A. Abedini, F. Torabi, Phase behaviour of CO_2-brine and CO_2-oil systems for CO_2 storage and enhanced oil recovery: experimental studies, Energy Procedia 63 (2014) 5631–5645. https://doi.org/10.1016/j.egypro.2014.11.596.

[20] R. M. Enick, S. M. Klara, Effects of CO2 solubility in brine on the compositional simulation of CO2 floods, SPE Reservoir Eng. 7 (1992) 253–258. https://doi.org/10.2118/20278-PA.

[21] Z. Li, M. Dong, S. Li, L. Dai, Densities and solubilities for binary systems of carbon dioxide + water and carbon dioxide + brine at 59°C and pressures to 29 MPa, J. Chem. Eng. Data 49 (2004) 1026–1031. https://doi.org/10.1021/je049945c.

[22] J. P. Ennis-King, L. Paterson, Role of convective mixing in the long-term storage of carbon dioxide in deep saline formations, SPE J. 10 (2005) 349–356. https://doi.org/10.2118/84344-PA.

[23] Z. Duan, R. Sun, An improved model calculating CO_2 solubility in pure water and aqueous NaCl solutions from 273 to 533 K and from 0 to 2000 bar, Chem. Geol. 193 (2003) 257–271. https://doi.org/10.1016/S0009-2541(02)00263-2.

[24] Z. Duan, R. Sun, C. Zhu, I.-M. Chou, An improved model for the calculation of CO_2 solubility in aqueous solutions containing Na^+, K^+, Ca^{2+}, Mg^{2+}, Cl^-, and SO_4^{2-}, Mar. Chem. 98 (2006) 131–139. https://doi.org/10.1016/j.marchem.2005.09.001.

[25] N. Spycher, K. Pruess, J. Ennis-King, CO_2-H_2O mixtures in the geological sequestration of CO_2. I. Assessment and calculation of mutual solubilities from 12 to 100°C and up to 600 bar, Geochim. Cosmochim. Acta 67 (2003) 3015–3031. https://doi.org/10.1016/S0016-7037(03)00273-4.

[26] N. Spycher, K. Pruess, CO_2-H_2O mixtures in the geological sequestration of CO_2. II. Partitioning in chloride brines at $12 - 100$°C and up to 600 bar, Geochim.

Cosmochim. Acta 69 (2005) 3309–3320. https://doi.org/10.1016/j.gca.2005.01.015.

[27] Z. Ziabakhsh-Ganji, H. Kooi, An equation of state for thermodynamic equilibrium of gas mixtures and brines to allow simulation of the effects of impurities in subsurface CO_2 storage, Int. J. Greenhouse Gas Control 11 (2012) S21–S34. https://doi.org/10.1016/j.ijggc.2012.07.025.

[28] G. M. Kontogeorgis, G. K. Folas, Thermodynamic Models for Industrial Applications: From Classical and Advanced Mixing Rules to Association Theories, John Wiley & Sons, Chichester, U.K., 2009.

[29] Y. Li, T. Zhang, S. Sun, X. Gao, Accelerating flash calculation through deep learning methods, J. Comput. Phys. 394 (2019) 153–165. https://doi.org/10.1016/j.jcp.2019.05.028.

[30] J. Kou, S. Sun, X. Wang, Linearly decoupled energy-stable numerical methods for multi-component two-phase compressible flow, SIAM J. Numer. Anal. 56 (2018) 3219–3248. https://doi.org/10.1137/17M1162287 and https://arxiv.org/abs/1712.02222.

[31] J. Kou, S. Sun, X. Wang, A novel energy factorization approach for the diffuse-interface model with peng-robinson equation of state, SIAM J. Sci. Comput. 42 (2020) B30–B56. https://doi.org/10.1137/19M1251230.

[32] D.-Y. Peng, D. B. Robinson, A new two-constant equation of state, Ind. Eng. Chem. Fundam. 15 (1976) 59–64. https://doi.org/10.1021/i160057a011.

[33] G. Soave, Equilibrium constants from a modified Redlich-Kwong equation of state, Chem. Eng. Sci. 27 (1972) 1197–1203. https://doi.org/10.1016/0009-2509(72)80096-4.

[34] I. Søreide, C. H. Whitson, Peng-Robinson predictions for hydrocarbons, CO_2, N_2, and H_2S with pure water and NaCl brine, Fluid Phase Equilib. 77 (1992) 217–240. https://doi.org/10.1016/0378-3812(92)85105-H.

[35] H. Sørensen, K. S. Pedersen, P. L. Christensen, Modeling of gas solubility in brine, Org. Geochem. 33 (2002) 635–642. https://doi.org/10.1016/S0146-6380(02)00022-

0.

[36] R. Masoudi, B. Tohidi, A. Danesh, A. C. Todd, A new approach in modelling phase equilibria and gas solubility in electrolyte solutions and its applications to gas hydrates, Fluid Phase Equilib. 215 (2004) 163–174. https://doi.org/10.1016/j.fluid.2003.08.009.

[37] A. Valtz, A. Chapoy, C. Coquelet, P. Paricaud, D. Richon, Vapour-liquid equilibria in the carbon dioxide-water system, measurement and modelling from 278.2 to 318.2 K, Fluid Phase Equilib. 226 (2004) 333–344. https://doi.org/10.1016/j.fluid.2004.10.013.

[38] A. Austegard, E. Solbraa, G. D. Koeijer, M. J. Mølnvik, Thermodynamic models for calculating mutual solubilities in H_2O-CO_2-CH_4 mixtures, Chem. Eng. Res. Des. 84 (2006) 781–794. https://doi.org/10.1205/cherd05023.

[39] J. Wu, J. M. Prausnitz, Phase equilibria for systems containing hydrocarbons, water, and salt: an extended Peng-Robinson equation of state, Ind. Eng. Chem. Res. 37 (1998) 1634–1643. https://doi.org/10.1021/ie9706370.

[40] P. Raveendran, S. L. Wallen, Cooperative $C-H\cdots O$ hydrogen bonding in CO_2-Lewis base complexes: implications for solvation in supercritical CO_2, J. Am. Chem. Soc. 124 (2002) 12590–2599. https://doi.org/10.1021/ja0174635.

[41] M. S. Wertheim, Fluids with highly directional attractive forces. II. Thermodynamic perturbation theory and integral equations, J. Stat. Phys. 35 (1984) 35–47. https://doi.org/10.1007/BF01017363.

[42] G. M. Kontogeorgis, E. C. Voutsas, I. V. Yakoumis, D. P. Tassios, An equation of state for associating fluids, Ind. Eng. Chem. Res. 35 (1996) 4310–4318. https://doi.org/10.1021/ie9600203.

[43] E. Perfetti, R. Thiery, J. Dubessy, Equation of state taking into account dipolar interactions and association by hydrogen bonding: II—Modelling liquid-vapour equilibria in the H_2O-H_2S, H_2O-CH_4 and H_2O-CO_2 systems, Chem. Geol. 251 (2008) 50–57. https://doi.org/10.1016/j.chemgeo.2008.02.012.

[44] Z. Li, A. Firoozabadi, Cubic-plus-association equation of state for water-containing mixtures: is cross association necessary?, AIChE J. 55 (2009) 1803–1813. https://doi.org/10.1002/aic.11784.

[45] G. D. Pappa, C. Perakis, I. N. Tsimpanogiannis, E. C. Voutsas, Thermodynamic modeling of the vapor-liquid equilibrium of the CO_2/H_2O mixture, Fluid Phase Equilib. 284 (2009) 56–63. https://doi.org/10.1016/j.fluid.2009.06.011.

[46] F. Tabasinejad, R. G. Moore, S. A. Mehta, K. C. V. Fraassen, Y. Barzin, J. A. Rushing, K. E. Newsham, Water solubility in supercritical methane, nitrogen, and carbon dioxide: measurement and modeling from 422 to 483 K and pressures from 3.6 to 134 MPa, Ind. Eng. Chem. Res. 50 (2011) 4029–4041. https://doi.org/10.1021/ie101218k.

[47] I. Tsivintzelis, G. M. Kontogeorgis, M. L. Michelsen, E. H. Stenby, Modeling phase equilibria for acid gas mixtures using the CPA equation of state. part II: Binary mixtures with CO_2, Fluid Phase Equilib. 306 (2011) 38–56. https://doi.org/10.1016/j.fluid.2011.02.006.

[48] M. Hajiw, J. Corvisier, E. E. Ahmar, C. Coquelet, Impact of impurities on CO_2 storage in saline aquifers: modelling of gases solubility in water, Int. J. Greenhouse Gas Control 68 (2018) 247–255. https://doi.org/10.1016/j.ijggc.2017.11.017.

[49] S. P. Tan, Y. Yao, M. Piri, Modeling the solubility of SO_2 + CO_2 mixtures in brine at elevated pressures and temperatures, Ind. Eng. Chem. Res. 52 (2013) 10864–10872. https://doi.org/10.1021/ie4017557.

[50] S. Chabab, P. Théveneau, J. Corvisier, C. Coquelet, P. Paricaud, C. Houriez, E. E. Ahmar, Thermodynamic study of the CO_2-H_2O-NaCl system: measurements of CO_2 solubility and modeling of phase equilibria using Soreide and Whitson, electrolyte CPA and SIT models, Int. J. Greenhouse Gas Control 91 (2019) 102825. https://doi.org/10.1016/j.ijggc.2019.102825.

[51] A. Hassanpouryouzband, M. V. Farahan, J. Yang, B. Tohidi, E. Chuvilin, V. Istomin, B. Bukhanov, Solubility of flue gas or carbon dioxide-nitrogen gas

mixtures in water and aqueous solutions of salts: experimental measurement and thermodynamic modeling, Ind. Eng. Chem. Res. 58 (2019) 3377–3394. https://doi.org/10.1021/acs.iecr.8b04352.

[52] L. Sun, G. M. Kontogeorgis, N. von Solms, X. Liang, Modeling of gas solubility using the electrolyte cubic plus association equation of state, Ind. Eng. Chem. Res. 58 (2019) 17555–17567. https://doi.org/10.1021/acs.iecr.9b03335.

[53] M. Hajiw, A. Chapoy, C. Coquelet, Hydrocarbons-water phase equilibria using the CPA equation of state with a group contribution method, Can. J. Chem. Eng. 93 (2015) 432–442. https://doi.org/10.1002/cjce.22093.

[54] T. Wang, E. E. Ahmar, C. Coquelet, Alkane solubilities in aqueous alkanolamine solutions with CPA EoS, Fluid Phase Equilib. 434 (2017) 93–101. https://doi.org/10.1016/j.fluid.2016.11.025.

[55] T. Wang, E. E. Ahmar, C. Coquelet, G. M. Kontogeorgis, Improvement of the PR-CPA equation of state for modelling of acid gases solubilities in aqueous alkanolamine solutions, Fluid Phase Equilib. 471 (2018) 74–87. https://doi.org/10.1016/j.fluid.2018.04.019.

[56] T. Jindrová, J. Mikyška, A. Firoozabadi, Phase behavior modeling of bitumen and light normal alkanes and CO_2 by PR-EOS and CPA-EOS, Energy Fuels 30 (2016) 515–525. https://doi.org/10.1021/acs.energyfuels.5b02322.

[57] O. Polívka, J. Mikyška, Compositional modeling in porous media using constant volume flash and flux computation without the need for phase identification, J. Comput. Phys. 272 (2014) 149–169. https://doi.org/10.1016/j.jcp.2014.04.029.

[58] H. Yang, S. Sun, Y. Li, C. Yang, A fully implicit constraint-preserving simulator for the black oil model of petroleum reservoirs, J. Comput. Phys. 396 (2019) 347–363. https://doi.org/10.1016/j.jcp.2019.05.038.

[59] H. Chen, J. Kou, S. Sun, T. Zhang, Fully mass-conservative impes schemes for incompressible two-phase flow in porous media, Comput. Methods Appl. Mech. Eng. 350 (2019) 641–663. https://doi.org/10.1016/j.cma.2019.03.023.

[60] G. Zhu, J. Kou, B. Yao, Y. shu Wu, JunYao, S. Sun, Thermodynamically consistent modelling of two-phase flows with moving contact line and soluble surfactants, J. Fluid Mech. 879 (2019) 327–359. https://doi.org/10.1017/jfm.2019.664.

[61] J. Mikyška, A. Firoozabadi, Investigation of mixture stability at given volume, temperature, and number of moles, Fluid Phase Equilib. 321 (2012) 1–9. https://doi.org/10.1016/j.fluid.2012.01.026.

[62] T. Jindrová, J. Mikyška, Fast and robust algorithm for calculation of two-phase equilibria at given volume, temperature, and moles, Fluid Phase Equilib. 353 (2013) 101–114. https://doi.org/10.1016/j.fluid.2013.05.036.

[63] J. Kou, S. Sun, A stable algorithm for calculating phase equilibria with capillarity at specified moles, volume and temperature using a dynamic model, Fluid Phase Equilib. 456 (2018) 7–24. https://doi.org/10.1016/j.fluid.2017.09.018.

[64] D. V. Nichita, Fast and robust phase stability testing at isothermal-isochoric conditions, Fluid Phase Equilib. 447 (2017) 107–124. https://doi.org/10.1016/j.fluid.2017.05.022.

[65] D. V. Nichita, New unconstrained minimization methods for robust flash calculations at temperature, volume and moles specifications, Fluid Phase Equilib. 466 (2018) 31–47.

[66] D. V. Nichita, Volume-based phase stability analysis including capillary pressure, Fluid Phase Equilib. 492 (2019) 145–160. https://doi.org/10.1016/j.fluid.2019.03.025.

[67] V. F. Cabral, M. Castier, F. W. Tavares, Thermodynamic equilibrium in systems with multiple adsorbed and bulk phases, Chem. Eng. Sci. 60 (2005) 1773–1782. https://doi.org/10.1016/j.ces.2004.11.007.

[68] Z. Qiao, S. Sun, Two-phase fluid simulation using a diffuse interface model with Peng-Robinson equation of state, SIAM J. Sci. Comput. 36 (2014) B708–B728. https://doi.org/10.1137/130933745.

[69] L. Travalloni, M. Castier, F. W. Tavares, Phase equilibrium of fluids confined in

porous media from an extended Peng-Robinson equation of state, Fluid Phase Equilib. 362 (2014) 335–341. https://doi.org/10.1016/j.fluid.2013.10.049.

[70] S. Luo, J. L. Lutkenhaus, H. Nasrabadi, Multiscale fluid-phase-behavior simulation in shale reservoirs using a pore-size-dependent equation of state, SPE Reservoir Eval. Eng. 21 (2018) 806–820. https://doi.org/10.2118/187422-MS.

[71] Y. Li, J. Kou, S. Sun, Thermodynamically stable two-phase equilibrium calculation of hydrocarbon mixtures with capillary pressure, Ind. Eng. Chem. Res. 57 (2018) 17276–17288. https://doi.org/10.1021/acs.iecr.8b04308.

[72] S. Sun, Darcy-scale phase equilibrium modeling with gravity and capillarity, J. Comput. Phys. 399 (2019) 108908. https://doi.org/10.1016/j.jcp.2019.108908.

[73] T. Jindrová, J. Mikyška, Phase equilibria calculation of CO_2-H_2O system at given volume, temperature, and moles in CO_2 sequestration, Int. J. Appl. Math. 45 (2015).

[74] G. M. Kontogeorgis, I. V. Yakoumis, H. Meijer, E. Hendriks, T. Moorwood, Multicomponent phase equilibrium calculations for water-methanol-alkane mixtures, Fluid Phase Equilib. 158 (1999) 201–209. https://doi.org/10.1016/S0378-3812(99)00060-6.

[75] M. L. Michelsen, Robust and efficient solution procedures for association models, Ind. Eng. Chem. Res. 45 (2006) 8449–8453. https://doi.org/10.1021/ie060029x.

[76] M. L. Michelsen, E. M. Hendriks, Physical properties from association models, Fluid Phase Equilib. 180 (2001) 165–174. https://doi.org/10.1016/S0378-3812(01)00344-2.

[77] K. A.-P. E. Stenby, A. Fredenslund, Prediction of high-pressure gas solubilities in aqueous mixtures of electrolytes, Ind. Eng. Chem. Res. 30 (1991) 2180–2185. https://doi.org/10.1021/ie00057a019.

[78] H. Haghighi, A. Chapoy, B. Tohidi, Freezing point depression of electrolyte solutions: experimental measurements and modeling using the cubic-plus-association equation of state, Ind. Eng. Chem. Res. 47 (2008) 3983–3989.

https://doi.org/10.1021/ie800017e.

[79] L. M. Pereira, A. Chapoy, R. Burgass, B. Tohidi, Interfacial tension of CO_2+brine systems: experiments and predictive modelling, Adv. Water Resour. 103 (2017) 64–75. https://doi.org/10.1016/j.advwatres.2017.02.015.

[80] V. S. Patwardhan, A. Kumar, A unified approach for prediction of thermodynamic properties of aqueous mixed-electrolyte solutions. part I: Vapor pressure and heat of vaporization, AIChE J. 32 (1986) 1419–1428. https://doi.org/10.1002/aic.690320903.

[81] J. Mikyška, A. Firoozabadi, A new thermodynamic function for phase-splitting at constant temperature, moles, and volume, AIChE J. 57 (2011) 1897–1904. https://doi.org/10.1002/aic.12387.

[82] A. Aasen, M. Hammer, G. Skaugen, J. P. Jakobsen, Ø. Wilhelmsen, Thermodynamic models to accurately describe the PVTxy-behavior of water/carbon dioxide mixtures, Fluid Phase Equilib. 442 (2017) 125–139. https://doi.org/10.1016/j.fluid.2017.02.006.

[83] Q. Duan, V. K. Gupta, S. Sorooshian, Shuffled complex evolution approach for effective and efficient global minimization, J. Optim. Theory Appl. 76 (1993) 501–521. https://doi.org/10.1007/BF00939380.

[84] G. M. Kontogeorgis, M. L. Michelsen, G. K. Folas, S. Derawi, N. von Solms, E. H. Stenby, Ten years with the CPA (Cubic-Plus-Association) equation of state. Part 1. Pure compounds and self-associating systems, Ind. Eng. Chem. Res. 45 (2006) 4855–4868. https://doi.org/10.1021/ie051305v.

[85] G. M. Kontogeorgis, M. L. Michelsen, G. K. Folas, S. Derawi, N. von Solms, E. H. Stenby, Ten years with the CPA (Cubic-Plus-Association) equation of state. Part 2. Cross-associating and multicomponent systems, Ind. Eng. Chem. Res. 45 (2006) 4869–4878. https://doi.org/10.1021/ie051306n.

[86] G. K. Folas, J. Gabrielsen, M. L. Michelsen, E. H. Stenby, G. M. Kontogeorgis, Application of the Cubic-Plus-Association (CPA) equation of state

to cross-associating systems, Ind. Eng. Chem. Res. 44 (2005) 3823–3833. https://doi.org/10.1021/ie048832j.

[87] A. Firoozabadi, Thermodynamics and Applications of Hydrocarbon Energy Production, McGraw Hill Professional, New York, 2015.

[88] R. Wiebe, V. L. Gaddy, Vapor phase composition of carbon dioxide-water mixtures at various temperatures and at pressures to 700 atmospheres, J. Am. Chem. Soc. 63 (1941) 475–477. https://doi.org/10.1021/ja01847a030.

[89] J. A. Briones, J. C. Mullins, M. C. Thies, B.-U. Kim, Ternary phase equilibria for acetic acid-water mixtures with supercritical carbon dioxide, Fluid Phase Equilib. 36 (1987) 235–246. https://doi.org/10.1016/0378-3812(87)85026-4.

[90] T. Nakayama, H. Sagara, K. Arai, S. Saito, High pressure liquid-liquid equilibria for the system of water, ethanol and 1,1-difluoroethane at 323.2 K, Fluid Phase Equilib. 38 (1987) 109–127. https://doi.org/10.1016/0378-3812(87)90007-0.

[91] A. Bamberger, G. Sieder, G. Maurer, High-pressure (vapor+liquid) equilibrium in binary mixtures of (carbon dioxide+water or acetic acid) at temperatures from 313 to 353 K, J. Supercrit. Fluids 17 (2000) 97–110. https://doi.org/10.1016/S0896-8446(99)00054-6.

[92] G. K. Anderson, Solubility of carbon dioxide in water under incipient clathrate formation conditions, J. Chem. Eng. Data 47 (2002) 219–222. https://doi.org/10.1021/je015518c.

[93] D. Koschel, J.-Y. Coxam, L. Rodier, V. Majer, Enthalpy and solubility data of CO_2 in water and NaCl(aq) at conditions of interest for geological sequestration, Fluid Phase Equilib. 247 (2006) 107–120. https://doi.org/10.1016/j.fluid.2006.06.006.

[94] S.-X. Hou, G. C. Maitland, J. M. Trusler, Measurement and modeling of the phase behavior of the (carbon dioxide +water) mixture at temperatures from 298.15 K to 448.15 K, J. Supercrit. Fluids 73 (2013) 87–96. https://doi.org/10.1016/j.supflu.2012.11.011.

[95] H. Guo, Y. Huang, Y. Chen, Q. Zhou, Quantitative raman spectroscopic mea-

surements of CO_2 solubility in nacl solution from (273.15 to 473.15) K at p = (10.0, 20.0, 30.0, and 40.0) MPa, J. Chem. Eng. Data 61 (2016) 466–474. https://doi.org/10.1021/acs.jced.5b00651.

[96] C. W. Meyer, A. H. Harvey, Dew-point measurements for water in compressed carbon dioxide, AIChE J. 61 (2015) 2913–2925. https://doi.org/10.1002/aic.14818.

[97] W. H. Rodebush, The freezing points of concentrated solutions and the free energy of solution of salts, J. Am. Chem. Soc. 40 (1918) 1204–1213. https://doi.org/10.1021/ja02241a008.

[98] H. F. Gibbard, A. F. Gossmann, Freezing points of electrolyte mixtures. I. Mixtures of sodium chloride and magnesium chloride in water, J. Solution Chem. 3 (1974) 385–393. https://doi.org/10.1007/BF00646479.

[99] D. L. Hall, S. M. Sterner, R. J. Bodnar, Freezing point depression of NaCl-KCl-H_2O solutions, Econ. Geol. 83 (1988) 197–202. https://doi.org/10.2113/gsecongeo.83.1.197.

[100] C. S. Oakes, R. J. Bodnar, J. M. Simonson, The system NaCl-$CaCl_2$-H_2O: I. The ice liquidus at 1 atm total pressure, Geochim. Cosmochim. Acta 54 (1990) 603–610. https://doi.org/10.1016/0016-7037(90)90356-P.

[101] W. M. Haynes, CRC Handbook of Chemistry and Physics, CRC Press, Boca Raton, 2016.

[102] H. C. Jones, J. N. Pearce, Dissociation as measured by freezing point lowering and by conductivity-bearing on the hydrate theory, Am. Chem. J. 38 (1907) 683.

[103] H. F. Gibbard, S.-L. Fong, Freezing points and related properties of electrolyte solutions. III. The systems NaCl-$CaCl_2$-H_2O and NaCl-$BaCl_2$-H_2O, J. Solution Chem. 4 (1975) 863–872. https://doi.org/10.1007/BF00649878.

[104] J. V. Leyendekkers, Structure of water in solutions in the subcooled region from freezing-point depressions, J. Chem. Soc., Faraday Trans. 1 82 (1986) 1663–1671. https://doi.org/10.1039/F19868201663.

[105] R. Sirbu, Thermodynamic studies of mixed aqueous solutions of binary

electrolytes of Na_2SO_4 and K_2SO_4, Thermochim. Acta 352 (2000) 1–10. https://doi.org/10.1016/S0040-6031(99)00429-3.

[106] B. Rumpf, H. Nicolaisen, C. Öcal, G. Maurer, Solubility of carbon dioxide in aqueous solutions of sodium chloride: experimental results and correlation, J. Solution Chem. 23 (1994) 431–448. https://doi.org/10.1007/BF00973113.

[107] W. Yan, S. Huang, E. H. Stenby, Measurement and modeling of CO_2 solubility in NaCl brine and CO_2-saturated NaCl brine density, Int. J. Greenhouse Gas Control 5 (2011) 1460–1477. https://doi.org/10.1016/j.ijggc.2011.08.004.

[108] P. J. Carvalho, L. M. Pereira, N. P. Gonçalves, A. J. Queimada, J. A. Coutinho, Carbon dioxide solubility in aqueous solutions of NaCl: measurements and modeling with electrolyte equations of state, Fluid Phase Equilib. 388 (2015) 100–106. https://doi.org/10.1016/j.fluid.2014.12.043.

[109] H. Zhao, M. V. Fedkin, R. M. Dilmore, S. N. Lvov, Carbon dioxide solubility in aqueous solutions of sodium chloride at geological conditions: experimental results at 323.15, 373.15, and 423.15 k and 150 bar and modeling up to 573.15 k and 2000 bar, Geochim. Cosmochim. Acta 149 (2015) 165–189. https://doi.org/10.1016/j.gca.2014.11.004.

[110] K. Jörn, S. Horstmann, K. Fischer, J. Gmehling, Experimental determination and prediction of gas solubility data for CO_2 + H_2O mixtures containing NaCl or KCl at temperatures between 313 and 393 K and pressures up to 10 MPa, Ind. Eng. Chem. Res. 41 (2002) 4393–4398. https://doi.org/10.1021/ie020154i.

[111] Á. P.-S. Kamps, E. Meyer, B. Rumpf, G. Maurer, Solubility of CO_2 in aqueous solutions of KCl and in aqueous solutions of K_2CO_3, J. Chem. Eng. Data 52 (2007) 817–832. https://doi.org/10.1021/je060430q.

[112] H. Zhao, R. M. Dilmore, S. N. Lvov, Experimental studies and modeling of CO_2 solubility in high temperature aqueous $CaCl_2$, $MgCl_2$, Na_2SO_4, and KCl solutions, AIChE J. 61 (2015) 2286–2297. https://doi.org/10.1002/aic.14825.

[113] C. F. Prutton, R. L. Savage, The solubility of carbon dioxide in calcium chloride-

water solutions at 75, 100, 120° and high pressures, J. Am. Chem. Soc. 67 (1945) 1550–1554. https://doi.org/10.1021/ja01225a047.

[114] D. Tong, J. P. M. Trusler, D. Vega-Maza, Solubility of CO_2 in aqueous solutions of $CaCl_2$ or $MgCl_2$ and in a synthetic formation brine at temperatures up to 423 K and pressures up to 40 MPa, J. Chem. Eng. Data 58 (2013) 2116–2124. https://doi.org/10.1021/je400396s.

[115] M. D. Bermejo, A. Martn, L. J. Florusse, C. J. Peters, M. J. Cocero, The influence of Na_2SO_4 on the CO_2 solubility in water at high pressure, Fluid Phase Equilib. 238 (2005) 220–228. https://doi.org/10.1016/j.fluid.2005.10.006.

[116] H. R. Corti, M. E. Krenzer, J. J. D. Pablo, J. M. Prausnitz, Effect of a dissolved gas on the solubility of an electrolyte in aqueous solution, Ind. Eng. Chem. Res. 29 (1990) 1043–1050. https://doi.org/10.1021/ie00102a014.

[117] Y. Liu, M. Hou, G. Yang, B. Han, Solubility of CO_2 in aqueous solutions of NaCl, KCl, $CaCl_2$ and their mixed salts at different temperatures and pressures, J. Supercrit. Fluids 56 (2011) 125–129. https://doi.org/10.1016/j.supflu.2010.12.003.

[118] Y. Marcus, Effect of ions on the structure of water: Structure making and breaking, Chem. Rev. 109 (2009) 1346–1370. https://doi.org/10.1021/cr8003828.

[119] R. Jacob, B. Z. Saylor, CO_2 solubility in multi-component brines containing NaCl, KCl, $CaCl_2$ and $MgCl_2$ at 297 K and 1–14 MPa, Chem. Geol. 424 (2016) 86–95. https://doi.org/10.1016/j.chemgeo.2016.01.013.

[120] H. Messabeb, F. Contamine, P. Cézac, J. P. Serin, C. Pouget, E. C. Gaucher, Experimental measurement of CO_2 solubility in aqueous $CaCl_2$ solution at temperature from 323.15 to 423.15 K and pressure up to 20 MPa using the conductometric titration, J. Chem. Eng. Data 62 (2017) 4228–4234. https://doi.org/10.1021/acs.jced.7b00591.

[121] M. Görgényi, J. Dewulf, H. V. Langenhove, K. Héberger, Aqueous salting-out effect of inorganic cations and anions on non-electrolytes, Chemosphere 65 (2006) 802–810. https://doi.org/10.1016/j.chemosphere.2006.03.029.